

Tracer hydrology of the data-scarce and heterogeneous Central American Isthmus

Ricardo Sánchez-Murillo^{1*}, Esquivel-Hernández, G.¹, Corrales-Salazar, L.¹, Castro-Chacón, L.², Durán-Quesada, A.M.³, Guerrero-Hernández, M.⁴, Delgado, V.⁵, Barberena, J.⁵, Montenegro-Rayó, K.⁵, Calderón, H.⁶, Chevez, C.⁷, Peña-Paz, T.⁸, García-Santos, S.⁸, Ortiz-Roque, P.⁹, Alvarado-Callejas, Y.¹⁰, Benegas, L.¹⁰, Hernández-Antonio, A.¹¹, Matamoros-Ortega, M.¹², Ortega, L.¹³, Terzer-Wassmuth, S.¹³.

¹Stable Isotope Research Group, UNA-SIL; Universidad Nacional, Heredia, Costa Rica

²Empresa de Servicios Públicos de Heredia, ESPH S.A., Heredia, Costa Rica

³Atmospheric, Planetary and Oceanic Physics Department, School of Physics and Center of Geophysical Research, University of Costa Rica, San José, Costa Rica

⁴Foundation for the Development of the Volcanic Central Cordillera, FUNDECOR, San José, Costa Rica

⁵Centro para la Investigación en Recursos Acuáticos de Nicaragua, CIRA/UNAN-Managua, Universidad Nacional Autónoma de Nicaragua, Managua, Nicaragua

⁶Institute of Geology and Geophysics, IGG-CIGEO, Universidad Nacional Autónoma de Nicaragua, Managua, Nicaragua

⁷Water Resources Department, Nicaraguan Institute of Territorial Studies, Managua, Nicaragua

⁸Instituto Hondureño de Ciencias de la Tierra, IHCIT, Universidad Nacional Autónoma de Honduras, Tegucigalpa, Honduras

⁹Servicio Autónomo Nacional de Acueductos y Alcantarillados, Gobierno de la República de Honduras, Tegucigalpa, Honduras

¹⁰Centro Agronómico Tropical de Investigación y Enseñanza, CATIE, Turrialba, Costa Rica

¹¹Servicios de Investigación Científica y Técnica SC, México

¹²Escuela de Biología, Universidad Nacional Autónoma de Honduras, Tegucigalpa, Honduras

¹³International Atomic Energy Agency, Isotope Hydrology Section, Vienna International Center, Vienna, Austria

*Corresponding Author: ricardo.sanchez.murillo@una.cr

Manuscript Components

Title: 10 words

Abstract: 255 words

Main text: 5,336 words (excluding acknowledgements and references)

Figures: 8 in color (figures caption text: 556 words)

Supplementary material: Datasets S1 (rainfall), S2 (surface water), S3 (groundwater)

Total references: 78

Running title: *Tracer hydrology in Central America*

Abstract

Numerous socio-economic activities depend on the seasonal rainfall and groundwater recharge cycle across the Central American Isthmus. Population growth and unregulated land use changes resulted in extensive surface water pollution and a large dependency on groundwater resources. This work combines stable isotope variations in rainfall, surface water, and groundwater of Costa Rica, Nicaragua, El Salvador, and Honduras to develop a regionalized rainfall isoscape, isotopic lapse rates, spatial-temporal isotopic variations, and air mass back trajectories determining potential mean recharge elevations, moisture circulation patterns, and surface water-groundwater interactions. Intra-seasonal rainfall modes resulted in two isotopically depleted incursions (W-shaped isotopic pattern) during the wet season and two enriched pulses during the Mid-Summer Drought and the months of the strongest trade

46 winds. Notable isotopic sub-cloud fractionation and near-surface secondary evaporation
47 were identified as common denominators within the Central American Dry Corridor.
48 Groundwater and surface water isotope ratios depicted the strong orographic separation
49 into the Caribbean and Pacific domains, mainly induced by the governing moisture
50 transport from the Caribbean Sea, complex rainfall producing systems across the N-S
51 mountain range, and the subsequent mixing with local evapotranspiration, and, to a
52 lesser degree, the eastern Pacific Ocean fluxes. Groundwater recharge was
53 characterized by a) depleted recharge in highland areas (72.3%), b) rapid recharge via
54 preferential flow paths (13.1%), and enriched recharge due to near-surface secondary
55 fractionation (14.6%). Median recharge elevation ranged from 1,104 to 1,979 m a.s.l.
56 These results are intended to enhance forest conservation practices, inform water
57 protection regulations, and facilitate water security and sustainability planning in the
58 Central American Isthmus.

59

60 **Keywords:** Central American Isthmus; Dry Corridor; ENSO; water stable isotopes;
61 groundwater recharge processes; water resources management.

62 1. Introduction

63 Central America (522,760 km²) is home to ~50 million inhabitants and highly
64 depends on groundwater extraction ($1.9 \times 10^4 \text{ m}^3 \text{ yr}^{-1}$) as a primary water resource, as a
65 result of the decline in quality and quantity of surface water resources (Ballesterro et al.,
66 2007; Hoekstra, 2018; Hund et al., 2018). During the last 100 years, the average
67 surface temperature has increased by 0.5 to 1.0°C and the number of warm days (% of
68 days when maximum daily temperature >90th percentile) rose by about 2.5% each
69 decade since the 1970s (Aguilar et al., 2005; Knutson et al., 2006), turning the region
70 into a prominent tropical hot-spot under future climate change scenarios (Giorgi, 2006).
71 Temperature increase in the region has been widely documented in independent
72 studies (Hidalgo and Alfaro, 2015; González et al., 2017; Lyra et al., 2017; Imbach et
73 al., 2018). The increasing trend of long-term droughts (> 5 months; Sheffield and Wood,
74 2008) poses a challenge for truly integrated water resources management in this region
75 (Foster MacDonald, 2014), particularly in light of a lack of national water balances.

76 Regional climate projections suggest relevant changes by 2050, including: 1) a
77 rainfall decrease (10-25%) during the wet season, 2) spatial extension of the area
78 affected by the Mid-Summer Drought (MSD; Magaña et al., 1999; Maldonado et al.,
79 2013; Maurer et al., 2017), and 3) positive trends in temperature and dry extreme
80 events, resulting in a net decrease of water availability (Imbach et al., 2018). In
81 particular, the Central America Dry Corridor (CADC) has received large attention in
82 recent years due to its ecohydrological vulnerability (Bouroncle et al., 2017). The CADC
83 is defined as a tropical dry forest region (dry season: mid-November to mid-May) on the
84 Pacific domain that extends from Chiapas (Mexico) to the western part of Costa Rica
85 and western provinces of Panama, also known as the Dry Arch of Panama (van der Zee
86 et al., 2012; Sánchez-Murillo and Birkel, 2016; FAO, 2017). The experience of recent
87 warm El Niño-Southern Oscillation (ENSO) events and resulting water scarcity has
88 promoted unified adaptation strategies regarding groundwater extraction for agriculture
89 (FAO, 2015). The dependence on seasonal rainfall and groundwater recharge for
90 agriculture, tourism and hydropower has further amplified the use of groundwater
91 resources.

92 Approximately 3.5 million people experienced food insecurity after suffering
93 major crop losses due to the prolonged warm ENSO-induced drought from 2014 to the
94 beginning of 2016 (FAO, 2016; Herrera and Ault, 2017). Therefore, a better
95 understanding of the factors that control rainfall patterns and the linkage to groundwater
96 recharge and surface discharge is an imperative task for Central American countries.
97 Robust and up-to-date hydrological information is required for stakeholders and
98 governmental agencies to prioritize efforts, resources, and regulations in watersheds or
99 regions, whereby potential droughts or extreme rainfall events could drastically disrupt
100 ecohydrological assemblages. However, in the absence of well-established and long-
101 term hydrometric networks in Central America, water stable isotopes are a reliable, fast,
102 and relative low-cost technique to study the interaction between rainfall inputs and
103 surface/groundwater connectivity in complex tropical landscapes (Sánchez-Murillo and
104 Durán-Quesada, 2018).

105 This work combines recent (2013-2018) and archive (sampling efforts since
106 1970s to early 2000s) stable isotope measurements in rainfall, surface water, and

107 groundwater of Costa Rica, Nicaragua, El Salvador, and Honduras. Historically, most of
108 the sampling efforts have been concentrated on the Pacific slope of Central America.
109 However, isotopic distributions within the Caribbean slope of Costa Rica are also
110 included to emphasize the relevance of the Caribbean Sea as a key moisture source. A
111 regionalized rainfall isoscape and isotopic lapse rate, air mass back trajectories, and
112 spatial-temporal isotopic variations were combined to determine potential mean
113 recharge elevations, moisture circulation patterns, and surface water-groundwater
114 connectivity. The results are intended to inform governmental institutions in Central
115 America and rise awareness regarding protection and conservation of critical recharge
116 zones. The present work also may contribute to the understanding of groundwater
117 recharge mechanisms in other tropical regions where isotopically-informed geospatial
118 models are becoming robust and more widely applied tools to improve water resources
119 planning (Taylor et al., 2013; Jasechko and Taylor, 2015; Sánchez-Murillo and Birkel,
120 2016; Dehaspe et al., 2018; Villegas et al., 2018; Munksgaard et al., 2019).

121 **2.1. Climatic features of Central America**

122 The regional climate can be analyzed in terms of the seasonal influence of four
123 main large-scale circulation patterns: 1) NE trade winds, 2) the latitudinal migration of
124 the Intertropical Convergence Zone (ITCZ), 3) cold continental surges, and 4) direct and
125 indirect influence of tropical cyclones (Waylen et al., 1996, Sáenz and Durán-Quesada,
126 2015). Those circulation patterns result from complex interactions among structures the
127 North Atlantic Subtropical High (NASH), the Western Hemisphere Warm Pool (WHWP,
128 Wang and Enfield 2001) dynamics, the seasonal migration of the ITCZ (Adam et al.,
129 2016) and the Caribbean Low-Level Jet (CLLJ, Amador 1998; Amador 2008). Figure 1
130 shows the seasonal patterns that characterize the above mentioned structures, with the
131 upper panel showing the evolution of the sea surface temperature (SST) and the
132 enhancement of the WHWP during the spring over the eastern tropical Pacific Ocean
133 (Fig. 1A) followed by the incursion of the WHWP in the Gulf of Mexico during the
134 summer months (Fig. 1B) and the further intensity decrease and dislocation to the inner
135 Caribbean after September (Fig. 1C). In a similar way, the months for which the CLLJ
136 exhibits its characteristic maximum and minimum peaks are shown in Figure 1. A
137 secondary peak is observed in February (Fig. 1D) with a distinguished zonal flow which

138 supports the development of the Papagayo jet to the Pacific due to wind funneling
139 across the northern Costa Rica plains and the Papagayo gap. The CLLJ primary peak
140 develops during summer (Fig. 2D) with a prominent northward branch that transports
141 moist air to northern Central America and the Gulf of Mexico. In contrast, a marked
142 minimum features the CLLJ by October (Fig. 3D), period in which a southwestern low-
143 level wind flow develops in the Pacific (known as the Choco Jet, Poveda and Mesa,
144 2000).

145 Rainfall in the region is defined by the intersection of large-scale circulation
146 patterns and local features and processes in which topography and vegetation cover
147 play a relevant role, resulting in two predominant rainfall maxima, one in May-June and
148 one in September-October. The rainfall maxima are interrupted by a relative minimum in
149 July-August known as the MSD which coincides with the CLLJ primary maximum, this
150 rainfall decrease is mainly characteristic of the Pacific slope of Central America as
151 noticed from the average annual cycle of rainfall shown in Figure 2. Moreover, rainfall
152 over the Pacific (as shown in Figure 2) also depicts a larger amount of rainfall when
153 compared to the Caribbean slope, which features as a spatially explicit broader rainfall
154 belt clearly identified as the ITCZ. It is also noteworthy that rainfall in the Caribbean has
155 a smoother annual cycle that features similar amounts of rainfall throughout the year.
156 Adding to the complexity of the precipitation system, the region also features the
157 development of mesoscale convective systems (MCS), large scale deep convective
158 systems known for their diurnal cycling over land and over ocean (Machado et al., 1998;
159 Mapes et al., 2003; Houze, 2004). MCS development peaks in the region during late
160 summer and early autumn months with a maximum occurrence over the Panama Bight
161 resulting from positive SST anomalies (Zuidema et al., 2006). These MCSs have a
162 variable life cycle that ranges from short lived (few hours) to long lived (20-24 hours)
163 systems and they are not only relevant for the accumulated rainfall but also form heavy
164 rainfall events. Fuchs et al. (2014) linked the formation of MCS with the ITCZ and with
165 Kelvin waves and traveling waves that led to heavy rainfall events. It is important to
166 highlight that the nature of rainfall amount, intensity and associated rain producing
167 systems that affect the region during the first and second legs of the rainy season are
168 different. As Durán-Quesada et al (2017) point out, the first leg of the rainy season is

169 more likely to have a larger influence of local surface interaction processes while the
170 second leg of the rainy season is more affected by large-scale dynamics.

171 Regional rainfall patterns are governed by the seasonal cyclicity of the SST
172 distribution. It is evident that the magnitude of ENSO and associated SST variations are
173 responsible for major changes in rainfall patterns with the shifting of the ITCZ being a
174 fundamental driver of drier conditions during warm ENSO events. During El Niño, the
175 more pronounced differences in warming between the northern and southern
176 hemisphere induce anomalous northward movement of the ITCZ. The shifting is more
177 prominent during boreal winter and is noticed as a southward shift of the ITCZ that can
178 reach 5°S during strong El Niño events (Schneider et al., 2014). The latitudinal shifting
179 along with the longitudinal variation of the ITCZ results in a decrease of deep convective
180 activity and negative precipitation anomalies along the Pacific slope of Central America.
181 The latter is a recurring pattern, particularly, in the CADC (Cid-Serrano et al., 2015).
182 Amador (2008) found that during warm ENSO phases, the CLLJ core is stronger,
183 resulting in an increase of zonal easterly trade winds. Easterlies intensification
184 increases the transport of moisture from the Caribbean and northern South America
185 (Durán-Quesada, 2012) and in turn decreases the moisture transport from the eastern
186 Pacific Ocean. Contrary to the Pacific side, the Caribbean domain of Central America is
187 wetter during the warm phase and drier during the cold phase (Cid-Serrano et al.,
188 2015). Hence, during warm ENSO events the dry-wet contrast of Central American
189 Pacific and Caribbean slopes becomes more marked, leading to severe drought in the
190 CADC and heavy rainfall extremes in the Caribbean.

191 **2.2. Geological generalities of Central America**

192 The Central American subduction zone is a complex deformation region
193 characterized by a rapid (70-90 mm/year) convergence rate of young (15-25 Ma)
194 oceanic lithosphere responding to the interaction of four plates: Caribbean, Cocos,
195 Nazca, and South American (Sak et al., 2009), whereby active tectonic deformation
196 continues to shape the Central American landscape. Geologically, Central America is
197 defined primarily by the northwest-trend of the Middle America trench and Central
198 American volcanic front (Bundschuh and Alvarado, 2007). According to the overall
199 tectonic setting, Central America is divided on the basis of crustal composition into two

200 main blocks: Northern Central America, a continental block consisting of Guatemala, El
201 Salvador, Honduras, and northern Nicaragua; and the southern Central America, an
202 uplifted oceanic slice consisting of Southern Nicaragua, Costa Rica, and Panama
203 (Dengo, 1973). The maximum elevation of volcanoes along Central America decreases
204 from Guatemala (Tajumulco volcano: 4,220 m a.s.l.) to Nicaragua (San Cristóbal
205 volcano: 1,745 m a.s.l.) with a decrease in crustal thickness (50 km to < 35 km) and
206 variations in the basement geology from continental to oceanic dominated
207 characteristics, whereas in Costa Rica, volcanoes elevation increases (Irazú volcano:
208 3,432 m a.s.l.) (~45 km) near the amagmatic gap, then decreases (~25 km) beneath
209 central Panamá (La Yeguada volcano: 1,297 m a.s.l.) (Leeman et al., 1994). Significant
210 groundwater recharge takes place within fractured and sloping aquifers in dormant or
211 active volcano complexes of Central America. However, the inherent complexity of
212 volcanic-originated aquifers, particularly, in steep and highly fractured groundwater
213 reservoirs, whereby lateral and vertical meteoric water mixing occurs (Madrigal-Solís et
214 al., 2017), challenges existing models of subsurface water flow paths and storage
215 (Delcamp et al., 2016) in such systems across the isthmus.

216 **3. Methods and Materials**

217 **3.1. Study Area**

218 The study area comprises four countries within the Central American Isthmus:
219 Costa Rica (both Pacific and Caribbean slopes), Nicaragua (Pacific slope), Honduras
220 (central and south Pacific slopes within the Choluteca river basin), and El Salvador
221 (south Pacific slope within the Bajo Lempa river basin). Since Central America shares a
222 common geomorphologic past (Coates and Obando, 1996), represented by the NW-SE
223 mountain range that divides the region into the Caribbean and Pacific slopes with
224 similar precipitation regimes (Alfaro, 2002) and soil characteristics, groundwater
225 recharge and surface runoff processes may be controlled by similar mechanisms, which
226 enforce the idea of using regionalized isotope approaches to elucidate dominant
227 hydrological processes to augment effective water resources management.

228

229

230

231 3.2. Stable isotope datasets

232 The rainfall stable isotope datasets is composed of 1,873 recent samples (2013-
233 2018) with weekly and daily collection frequencies, as part of concerted efforts between
234 the Stable Isotope Research Group (National University, Costa Rica, the Earth
235 Sciences Institute of Honduras (Autonomous National University, Honduras), the
236 Research Center for Aquatic Resources of Nicaragua (National Autonomous University
237 of Nicaragua, Managua), the Tropical Agricultural Research and Higher Education
238 Center (CATIE, Costa Rica), and the Water Center for Latin America and the Caribbean
239 (Monterrey, México), with the support of the Isotope Hydrology Section of the
240 International Atomic Energy Agency (Vienna, Austria). Rainfall was collected using
241 passive collectors (Palmex Ltd., Zagreb, Croatia) (Gröning et al., 2012). Samples were
242 collected in 15-50 mL HDPE-lined caps bottles, filled with no head space when
243 permitted, and stored at 5°C until analysis. The ongoing isotope monitoring network in
244 precipitation provides a better spatial distribution across different climatic zones,
245 altitudes, and biomes of Central America (Fig. 3A).

246 The rainfall stable isotope dataset is divided as follows: a) Costa Rica Caribbean
247 slope (N=834; 2014-2018, ~30 km from the Caribbean coast); b) Costa Rica Pacific
248 slope (N=472; 2013-2018, at the Central Valley of Costa Rica); c) Nicaragua Caribbean
249 slope (N=48; 2017, near the Caribbean coast at Bluefields); d) Nicaragua Pacific slope
250 (N=190; 2016-2018, at Managua); e) Honduras (N=232; 2018, within the Tegucigalpa
251 Valley and southern Pacific slope); and f) El Salvador (N=94; 2016-2017, within the
252 southern Pacific slope) (Fig. 3A).

253 Similarly, the groundwater and surface water stable isotope datasets are
254 composed of recent and archived measurements as follows: a) El Salvador (N=38;
255 2016-2017, within the southern Pacific slope), b) Honduras (N=391; 2018, within the
256 Tegucigalpa Valley and north central region), c) Nicaragua (N=1,005; from 1970s to
257 early 2000s and 2016, across the entire Pacific slope), d) Costa Rica Caribbean slope
258 (N=354; 2014-2018), and e) Costa Rica Pacific slope (N=934; 2014-2018) (Fig. 3B and
259 3C). Recent sampling campaigns targeted base flow conditions with the aim of
260 obtaining representative mean annual isotopic values at a high spatial resolution
261 (Sánchez-Murillo and Birkel, 2016). Groundwater water samples were collected from

262 automated and artisanal drinking water wells and perennial spring systems. Well valves
263 were opened, and the water flowed for 10 minutes prior to sample collection to avoid
264 stagnant water, in case the well was turned off for longer time periods according to local
265 well operators. Surface waters were exclusively collected at the flowing sections of
266 streams to avoid stagnant ponds with strong evaporative signals. Both groundwater and
267 surface water samples were collected in 15-50 mL HDPE-lined caps bottles, filled with
268 no head space, and stored at 5°C until analysis.

269 **3.3. Stable isotope analysis**

270 Stable isotope archives from IAEA data sources comprise multiple laboratories,
271 whereby samples were analyzed by Isotope Ratio Mass Spectrometry (IRMS) before
272 the advent of laser spectroscopy. Recent stable isotope analyses were conducted at a)
273 the Stable Isotope Research Group facilities of the National University (Heredia, Costa
274 Rica) using a Cavity Ring Down Spectroscopy (CRDS) water isotope analyzer L2120-*i*
275 (Picarro, USA) and a LWIA-45-EP water isotope analyzer (Los Gatos, USA), b) the
276 Research Center for Aquatic Resources of Nicaragua (National Autonomous University
277 of Nicaragua, Managua) using a LWIA-45-EP water isotope analyzer (Los Gatos, USA),
278 and c) at the Water Center for Latin America and the Caribbean (Monterrey, México)
279 using a DLT-100 water isotope analyzer (Los Gatos, USA). Calibrated secondary
280 standards were used to normalize the results as well as to assess quality and drift
281 control procedures. $^{18}\text{O}/^{16}\text{O}$ and $^2\text{H}/^1\text{H}$ ratios are presented in the established delta
282 notation δ (‰), with reference to the VSMOW-SLAP scale. Deuterium excess was
283 calculated as $d\text{-excess} = \delta^2\text{H} - 8 \cdot \delta^{18}\text{O}$ (Dansgaard, 1954).

284 **3.4. HYSPLIT air mass back trajectories**

285 The influence of atmospheric trajectory and source meteorological conditions on
286 the subsequent stable isotope composition of precipitation was studied using the
287 HYSPLIT Lagrangian model (Stein et al., 2015) developed by the Air Resources
288 Laboratory (ARL) of National Oceanic and Atmospheric Administration (NOAA, USA).
289 The HYSPLIT model uses a three-dimensional Lagrangian air mass vertical velocity
290 algorithm to determine the average position of the air mass which is reported at an
291 hourly time-resolution over the trajectory (Soderberg et al., 2013). Air parcel trajectories
292 were modeled 48 hours backwards in time based on the proximity of the Caribbean Sea

293 and the Pacific Ocean. To compute a trajectory, the HYSPLIT model requires a starting
294 time (13:00 p.m. UTC, which corresponds to the sample collection time of 7:00 a.m. in
295 Costa Rica), location (-84.1091 W and 10.0004 N), and altitude (1,100 m a.s.l.,
296 Sánchez-Murillo et al., 2016a) as well as NOAA meteorological data files (e.g. GDAS,
297 global data assimilation system: 2006-present; Su et al., 2015). In total, 476 air mass
298 back trajectories were created and further divided into two main groups: the dry season
299 (January-April) and the wet season (May-December) to compare the main moisture
300 transport mechanisms across the Central American Isthmus.

301 **3.5. Central America rainfall isoscape**

302 A Central America rainfall isoscape (in the definition of Bowen et al. 2010) was
303 generated using data originating from the Global Network of Isotopes in Precipitation
304 (GNIP, IAEA/WMO 2018), using the methods presented by Terzer et al. (2013; RCWIP
305 – Regionalized Cluster-Based Water Isotope Prediction). This approach is based on a
306 combined approach of regressing the mean $\delta^{18}\text{O}$ and $\delta^2\text{H}$ at a GNIP station against
307 geographical and climatic regressors and applying the resulting function onto gridded
308 climate data. The station-based residuals were then interpolated onto the resulting
309 regression grid to account for local anomalies not accounted for by the regression.
310 However, as the geographical domain was constrained, and given the rather coarse
311 spatial resolution of this isoscape grids (10 arc-minutes), two major modifications were
312 applied: (a) given the relative climatic homogeneity of the region, the input data was
313 constrained to an area between 0° and 30°N and 70° and 110°W rather than applying
314 any clustering, and (b) WorldClim2 gridded climate data (Fick and Hijmans, 2017) at 30
315 arc-seconds resolution were used, although the best-fit regression was determined on
316 geographical regressors (latitude=LAT and altitude=ALT) alone. One of the particular
317 caveats of the prediction technique was however, that the records used to derive the
318 station-based mean isotopic values were spatially and temporally inhomogeneous as a
319 result of data scarcity (cf. also Bowen et al. 2010 and Terzer et al. 2013 on the issue),
320 which will require future re-assessments based on longer time series.

321

322

323 3.6. Potential mean recharge elevation and rainfall-groundwater connectivity

324 Mean $\delta^{18}\text{O}$ annual values of 57 historical GNIP and recent stations (elevation
325 range from 100 to 3,400 m a.s.l.) were used to construct a regionalized isotopic lapse
326 rate for the Pacific slope of Central America (*Adj. $r^2=0.32$, p -value <0.001 , ~ -1.0 ‰ $\delta^{18}\text{O}$*
327 *per km of elevation with 95% confidence intervals*). Since most of Central America's
328 population (Fig. 3D) and water scarcity issues are located on the Pacific slope, this
329 analysis does not include the Caribbean domain information. The isotopic lapse rate
330 was used to calculate potential mean recharge elevations (in m a.s.l.) under the
331 assumption that groundwater isotope ratios are representative of mean annual recharge
332 conditions. Furthermore, a rainfall to groundwater isotopic diagram was constructed
333 following Jasechko and Taylor (2015) to estimate the isotopic recharge bias across the
334 Central American Isthmus. Mean $\delta^{18}\text{O}$ annual values in rainfall were extracted from the
335 regionalized isoscape and rainfall to groundwater isotope ratios (P/GW [-]) were
336 calculated to evaluate groundwater recharge mechanisms. A P/GW > 1 indicates sites
337 where infiltrated water is susceptible to near surface secondary evaporation, while a
338 P/GW ratio < 1 points towards recharge originating from more intense and more
339 depleted rainfalls at high altitudes. A P/GW ~ 1 indicates a rapid recharge via
340 preferential flow paths (Sánchez-Murillo and Birkel, 2016).

341 A Kruskal-Wallis non-parametric analysis of variance on ranks (Kruskal and
342 Wallis, 1952) was applied to test if there was stochastic dominance of one group
343 over another regarding $\delta^{18}\text{O}$ (‰), $\delta^2\text{H}$ (‰), *d*-excess (‰), and MRE values. A significant
344 difference was determined ($P<0.001$) when median values among the groups
345 (countries) were greater than expected by chance. In addition, for all groups having a
346 significant difference, an all pairwise multiple comparison procedure was applied using
347 Dunn's method (Dunn, 1961) to test if there is evidence of stochastic dominance
348 between the samples ($P<0.05$). Dunn's method approximates exact rank-sum test
349 statistics by using the median rankings of the results in each group from the previous
350 Kruskal-Wallis non-parametric test and provides an inference in median ranks in each
351 group. Statistical and graphical analysis was performed using the open source statistical
352 R language and packages (R Development Core Team, 2014). All maps were
353 developed in ArcGIS 10.5 (ESRI, USA).

354 4. Results and Discussion

355 4.1. Regional rainfall isotope variability and moisture transport

356 The regression equations used as suitable predictions for the annual mean $\delta^{18}\text{O}$
357 and $\delta^2\text{H}$ in the Central America region (RMSE on $\delta^{18}\text{O}$ =0.77 and $\delta^2\text{H}$ =6.4) are:

$$358 \quad \delta^{18}\text{O} = 0.078 \cdot \text{LAT} - 0.0023 \cdot \text{ALT} - 5.447 \quad (R^2 = 0.81, p - \text{value} < 0.01) \quad (\text{Eq. 1})$$

$$359 \quad \delta^2\text{H} = 0.585 \cdot \text{LAT} - 0.0174 \cdot \text{ALT} - 33.639 \quad (R^2 = 0.79, p - \text{value} < 0.01) \quad (\text{Eq. 2})$$

360 Mean annual $\delta^{18}\text{O}$ in rainfall ranged from -3.65‰ to -12.14‰ across the Central
361 American Isthmus (Fig. 4A). Enriched rainfall was commonly observed in the Caribbean
362 lowlands, whereas depleted rainfall was observed across the Pacific slope of the main
363 mountain ranges from Guatemala (i.e. Sierra Madre) to the Costa Rica/Panama border
364 (i.e. Talamanca range). Figure 4B shows a representative analysis of air mass back
365 trajectories in the Central American Isthmus using a daily sampling station in central
366 Costa Rica (2013-2017). During the 2013-2017 period, conditions featured weak as well
367 as strong El Niño situations, with a very strong El Niño developing in 2015-2016. The
368 dominance of El Niño in that period was associated with an anomalous migration of the
369 ITCZ and a weaker CLLJ during winter time. Warmer waters favored evaporation in the
370 Pacific and the intensification of the southwesterly flow, which, given weaker easterlies,
371 allowed for increased moisture transport from the tropical Pacific to the isthmus. The
372 latter is in good agreement with previous results from Durán-Quesada (2012) which
373 showed a positive, non-lagged correlation of 0.79 between the eastern tropical Pacific
374 Ocean moisture transport to Central America and El Niño 3.4 index during February.
375 The intensification of moisture transport to the isthmus under El Niño is consistent
376 across the region with a larger transport to the northernmost part of the region (Durán-
377 Quesada et al., 2017). The isoscape in Figure 4A, shows a remarkable spatial variability
378 of $\delta^{18}\text{O}$, with an enriched composition over coastal areas as a result of rainfall forming
379 at lower altitudes and a low-level convergence favored by higher temperatures. The
380 northern portion of the CADC remarkably features more enriched values (as well as
381 higher elevations), associated to water vapor coming from an environment of larger
382 evaporation as observed during warm ENSO events in the area. Local
383 evapotranspiration and Pacific moisture transport played a significant role in the vapor

384 budget during the wet season (Fig. 4B). Overall, as water vapor encounters the main
385 mountain range, orographic distillation and convergence increased, resulting in depleted
386 rainfall across the Pacific domain. Orographic depressions enhanced the incursion of
387 enriched-type rainfall across the highlands of the Pacific slope, with subsequent mixing
388 of depleted and enriched percolation into the mountainous aquifers (Sánchez-Murillo et
389 al., 2016b; Ramírez-Leiva et al., 2017; Esquivel-Hernández et al., 2018).

390 Recent daily and weekly rainfall isotope measurements resulted in highly
391 significant LMWLs (Fig. 5A). Caribbean LMWLs (Nicaragua and Costa Rica) exhibited
392 similar conditions relative to the Global Meteoric Water Line (GMWL; Craig, 1961),
393 whereas stations located on the Pacific slope, consistently, exhibited lower slopes
394 (7.42-7.88) and intercepts (4.99-8.42) (Fig. 5A). Sánchez-Murillo et al. (2016a) reported
395 that sub-cloud evaporation is a key driver controlling rainfall isotope composition within
396 the Pacific slope of Central America. Non-equilibrium processes under an unsaturated
397 condition below the cloud base, enhance the net transfer of water molecules from the
398 falling drops to the surrounding air (Kong and Pang, 2016; Salamalikis et al., 2016;
399 Crawford et al., 2017; Graf et al., 2018), resulting in enriched surface rainfall. The latter
400 process is a potential common feature within the CADC, whereby recent warm ENSO-
401 induced droughts decreased rainfall amounts and intensities as well as promoting more
402 intense warming and unsaturated atmosphere conditions during rainfall events (Jimenez
403 et al., 2018; Muñoz-Jimenez et al., 2018).

404 Figure 5B shows a time series of rainfall isotope during 2017-2018 in Costa Rica,
405 Nicaragua, and Honduras. In general, climate seasonality from dry (Jan-Apr) to wet
406 season (May-December) was characterized by a W-shaped isotopic pattern (Sánchez-
407 Murillo et al., 2019). The latter is in consistency with the pronounced intra-seasonal
408 rainfall variations that results in two depleted incursions during the wet season and
409 enriched pulses during the MSD and the peak of the CLLJ (Fig. 5B). These trends were
410 amplified within the CADC, whereas in the Caribbean domain the isotopic composition
411 was less variable throughout the year. Differences found when comparing $\delta^{18}\text{O}$ values
412 for the three countries reflected the larger influence of the ITCZ for Costa Rica as well
413 as the relevance of rainfall events derived from highly energetic systems and a wetter
414 environment that results from a supersaturated atmosphere. Meanwhile, seasonality of

415 $\delta^{18}\text{O}$ for Nicaragua is described by drier conditions in comparison to Costa Rica.
416 Honduras showed a rather special case as the influence of the ITCZ up north is lower
417 compared to Costa Rica and the depleted values observed with a depleted composition
418 in October show the influence of cyclonic activity and the activity of transients, which
419 despite a similar isotopic composition as identified from the ITCZ passage denote the
420 influence of a different process that also generates deep convection.

421 **4.2. Rainfall and surface/groundwater connectivity**

422 Figure 6 shows a series of scattered and box plots in rainfall, groundwater, and
423 surface water. Orographic isotope separation between the Caribbean and Pacific slopes
424 was clearly depicted in Costa Rica, whereby rainfall medians differed by 5.3‰ in $\delta^{18}\text{O}$.
425 Rainfall from the Caribbean lowlands of Nicaragua and Costa Rica exhibited a similar
426 enrichment trend. Notably, the rainfall median values in the northern portion of the
427 CADC (Nicaragua, El Salvador, and Honduras) were significantly greater than the
428 Pacific slope of Costa Rica (median values ranging from -3.9 to -4.5‰ in $\delta^{18}\text{O}$) (Fig.
429 6A). Similarly, *d*-excess variations indicated a mixture of enhanced moisture recycling
430 (Caribbean Sea-derived moisture) and below cloud fractionation, particularly, in
431 Nicaragua and El Salvador (Fig. 6D).

432 The most $\delta^{18}\text{O}$ depleted groundwater was reported in the Pacific slope of Costa
433 Rica (median=-7.9‰), while groundwater isotope values of Honduras (median=-7.1‰)
434 and Nicaragua (median=-6.8‰) presented similar median values. The most enriched
435 groundwater was reported in the south Pacific slope of El Salvador (median=-6.0‰)
436 (Fig. 6B). The significantly low *d*-excess values in groundwater of Nicaragua evidenced
437 the strong connectivity between lakes and groundwater reservoirs as well as potential
438 surface secondary evaporation during recharge processes (Fig. 6E).

439 Overall, surface waters across the isthmus exhibited a clear enrichment trend,
440 reflected in the low *d*-excess median values. In Nicaragua, the large presence of
441 sampled lakes, biased the median value towards -1.74‰ in $\delta^{18}\text{O}$ with a broad spectrum
442 of isotope values (from +5 to -10‰). In Costa Rica, El Salvador, and Honduras surface
443 water isotope values revealed a close relationship with the median values of
444 groundwater (median values ranging from -6.1 to -7.1‰ in $\delta^{18}\text{O}$) (Fig. 6C).

445

4.3. Regional groundwater recharge assessment

The complex topography of Central America and the existence of two large water pools nearby (i.e. Caribbean Sea and Pacific Ocean) provide a unique scenario to test the water vapor distillation/elevation effect on groundwater isotopic composition. A compilation of 57 historical and recent monitoring rainfall stations (>100 m a.s.l.) resulted in a significant regionalized isotopic lapse rate of $\sim 1.0\text{‰}$ in $\delta^{18}\text{O}$ per 1 km of elevation (*Adj. r^2* =0.32; *p*-value<0.001) (Fig. 7A). Previous studies have reported similar isotopic lapse rates for particular countries in the region (Lachniet et al., 2007; Wassenaar et al., 2009; Sánchez-Murillo et al., 2013; Windhorst et al., 2013; Sánchez-Murillo and Birkel, 2016). The rain-out effect over the Caribbean slope was a result of the direct influence of the trade winds and nearby moisture transport from the Caribbean Sea (isotopic lapse rate not included; see Sánchez-Murillo and Birkel, 2016), whereas in the Pacific slope the combination of the rain shadow effect, more complex orography and biomes, and deep convective activity throughout the wet season, resulted in a weaker elevation trend (Fig. 7A).

Figure 7B shows the probabilistic density distribution of the isotope-derived MRE across the Pacific slope of the isthmus. Median MRE were not significantly different between Nicaragua ($1,024 \pm 15$ m a.s.l.), Honduras ($1,289 \pm 27$ m a.s.l.), and El Salvador ($1,104 \pm 119$ m a.s.l.). Costa Rica exhibited a positive skewed distribution with a median MRE of $1,979 \pm 30$ m a.s.l. The bimodal distribution of Costa Rica in the MRE determination is affected by the strong influence of enriched-type rainfall across high elevation topographic depressions (i.e. a NE moisture pass) resulting in inverse altitude effects (Sánchez-Murillo et al., 2016b). Overall, MRE across the northern portion of the CADC indicated infiltration below 2,000 m a.s.l., while higher elevations were found in the central and southern Pacific domain of Costa Rica.

Figure 8A shows a rainfall to groundwater isotopic diagram to assess groundwater recharge bias (Jasechko and Taylor, 2015; Sánchez-Murillo and Birkel, 2016). In general, groundwater recharge was characterized by three distinct mechanisms: a) depleted recharge at the highland areas (72.3%), b) rapid recharge via preferential flow paths (13.1%), and enriched recharge due to secondary fractionation in the rainfall generation and near surface enrichment by soil matrix attenuation, small

477 recharge rates, and interaction with large scale lake systems (14.6%) (Fig. 8C).
478 Latitudinally, P/GW isotopic ratios indicated preferential recharge may occur along the
479 isthmus in highly fractured volcanic aquifers, whereas enriched recharge tends to
480 increase from 8° to 14°N and depleted high elevation recharge was favored towards
481 Costa Rica (Fig. 8B).

482 **5. Conclusions**

483 This work presented the first regional synthesis of the spatio-temporal isotopic
484 variability in four tropical countries: Costa Rica, Nicaragua, El Salvador and Honduras,
485 whereby decades of collaboration between IAEA and Member States established the
486 foundation of tracer Hydrology studies in the Central American Isthmus. Recent
487 sampling campaigns across the isthmus provided novel evidence of isotopic trends in
488 the hydrological cycle. In this region, considered a climate change 'hot spot', complex
489 rainfall and groundwater recharge mechanisms recurrently affected by ENSO events,
490 challenge water resources management. Due to limited hydrometric networks,
491 particularly, in monitoring groundwater levels and surface water discharge, rapid and
492 robust isotopic assessments may shed light on the understanding of hydrogeological
493 and meteorological processes.

494 Our results revealed a regionalized temporal pattern in the isotopic composition
495 of rainfall, with a remarkable enrichment towards the northern portion of the CADC.
496 Moisture transport was mainly governed by the semi-closed basin of the Caribbean
497 Sea, and to a lesser degree, inputs from the central Pacific Ocean and local
498 evapotranspiration fluxes were also attributed in the air mass back trajectory analysis.
499 Groundwater recharge was characterized by three main governing mechanisms: a)
500 depleted recharge at the highland areas, b) rapid recharge via preferential flow paths,
501 and enriched recharge due to near-surface secondary fractionation. Consistent low *d*-
502 excess values suggested a clear connection between surface water (i.e. rivers and
503 large-scale lakes) and groundwater reservoirs.

504 Significant temporal and spatial gaps invoke more systematic efforts that
505 accounts for better i) sampling gradients to improve isotopic lapse rates, ii) surface
506 water and groundwater sampling during baseflow regimes to characterize mean annual
507 conditions, iii) an urgent groundwater assessment in the CADC, and iv) characterization

508 of the poorly-sampled Caribbean lowland domain. Furthermore, the climatic and
509 hydrogeological similarities of the Central American isthmus should facilitate the
510 selection of sites for effective mid- to long-term monitoring efforts of isotopes in various
511 components of the water cycle, with resulting data that can be used to a) improve the
512 existing isoscape(s), triggering a positive feedback between prediction and observation
513 efforts, b) enhance ongoing forest conservation and land use practices, c) enforce
514 protection laws in critical recharge elevations, and d) guarantee water security and
515 sustainability of ~50 million inhabitants through the incorporation of tracer hydrology
516 insights in modelling assessments and decision making.

517 **Data availability statement**

518 The data that supports the findings of this study are available in the
519 supplementary material of this article.

520 **6. Acknowledgments**

521 This study was supported by International Atomic Energy Agency grants
522 COS/7/005, RC-19747, and RLA/7/024. A Joint Research Agreement (SIA-0378-14) by
523 the National University (Heredia, Costa Rica) and Empresa de Servicios Públicos de
524 Heredia (ESPH S.A.) was also fundamental. Funding from the Research Office of the
525 National University (Heredia, Costa Rica) through grants SIA-0482-13, SIA-0101-14,
526 SIA-0236-16, SIA-411-17, and SIA-414-17 was crucial for conducting sampling
527 campaigns across the isthmus. Support from the Isotope Network for Tropical
528 Ecosystem Studies (ISONet) funded by the University of Costa Rica Research Council
529 is recognized. The Research Center for Aquatic Resources of Nicaragua (National
530 Autonomous University of Nicaragua, Managua) thanks the support from the IAEA
531 Technical Cooperation project NIC/5/009. Acknowledgement to the European Union
532 through the Project WATERCLIMA LAC No. DCI-ENV 2014/350-470 executed by the
533 Tropical Agricultural Research and Higher Education Center (CATIE), coastal zones
534 management in El Salvador, as well as a sincere thanks to Alejandro Felix and Walter
535 Chacon for coordinating field work and to Jurgen Mahlkecht and Antonio Torres of the
536 Water Center for Latin America and the Caribbean for their valuable assistance in the

537 analysis of samples. FUNDECOR recognizes the funding from Water for the Future
538 within the Replenishment Project (Coca Cola FEMSA-TNC). The authors thank various
539 anonymous helping hands that contributed to rainfall, surface water, and groundwater
540 sampling in Central America.

541 7. References

542

543 1. Adam, O., Bischoff, T. and Schneider, T. 2016. Seasonal and interannual
544 variations of the energy flux equator and ITCZ. Part II: Zonally varying shifts of
545 the ITCZ. *Journal of Climate*, 29(20): 7281-7293. [https://doi.org/10.1175/JCLI-D-](https://doi.org/10.1175/JCLI-D-15-0710.1)
546 [15-0710.1](https://doi.org/10.1175/JCLI-D-15-0710.1)

547

548 2. Aguilar, R. et al. 2005. Changes in precipitation and temperature extremes in
549 Central America and northern South America, 1961–2003. *Geophysical*
550 *Research*, 110, D23107. <https://doi.org/10.1029/2005JD006119>

551

552 3. Alfaro, E. 2002. Some characteristics of the annual precipitation cycle in Central
553 America and their relationships with its surroundings tropical oceans. *Top.*
554 *Meteoro. Oceanog.* 9(2): 88-103. Accessible at:
555 <http://repositorio.ucr.ac.cr/handle/10669/15428>

556

557 4. Amador J. 2008. The intra-Americas seas low-level jet (IALLJ): Overview and
558 future research. *Ann. N. Y. Acad. Sci.*, 1146: 153-188.
559 <https://doi.org/10.1196/annals.1446.012>

560

561 5. Amador J. A. 1998. A climatic feature of the tropical Americas: The trade wind
562 easterly jet. *Meteorological and Oceanographical Topics*, 5(2): 91-102.

563

564 6. Ballesteros, M., Reyes, V., and Astorga, Y. 2007. Groundwater in Central
565 America: its importance, development and use, with reference to its role in
566 irrigated agriculture. Giordano, M. & Villholth, KG, The agricultural groundwater
567 revolution. Opportunities and threads to development. International water
568 Management Institute (IWMI), Colombo, Sri Lanka (2007): 100-128.
569 [http://funcagua.org.gt/wp-content/uploads/2018/06/Groundwater-in-Central-](http://funcagua.org.gt/wp-content/uploads/2018/06/Groundwater-in-Central-America-2007-et-al-Ballesteros.pdf)
570 [America-2007-et-al-Ballesteros.pdf](http://funcagua.org.gt/wp-content/uploads/2018/06/Groundwater-in-Central-America-2007-et-al-Ballesteros.pdf)

571

572 7. Bouroncle, C. et al. 2017. Mapping climate change adaptive capacity and
573 vulnerability of smallholder agricultural livelihoods in Central America: ranking
574 and descriptive approaches to support adaptation strategies. *Climatic Change*,
575 141(1): 123-137. <https://doi.org/10.1007/s10584-016-1792-0>

576

577 8. Bowen, G. J. 2010. Statistical and geostatistical mapping of precipitation water
578 isotope ratios, in: *Isoscapes: Understanding movement, pattern, and process on*
579 *Earth through isotope mapping*, edited by: West, J. B., Bowen, G. J., Dawson, T.

- 580 E., and Tu, K. P., Springer, London, 139–178. <https://doi.org/10.1007/978-90->
581 [481-3354-3_7](https://doi.org/10.1007/978-90-481-3354-3_7)
582
- 583 9. Bundschuh, J. and Alvarado, G.E. eds., 2007. Central America: Geology,
584 Resources and Hazards. CRC Press.
585
- 586 10. Cid-Serrano L, Ramírez SM, Alfaro EJ, Enfield DB. 2015. Analysis of the Latin
587 American west coast precipitation predictability using an ENSO index. *Atmósfera*,
588 28 (3):191-203. <https://doi.org/10.20937/ATM.2015.28.03.04>
589
- 590 11. Coates, A.G. and Obando, J.A. 1996. The geologic evolution of the Central
591 American Isthmus, In *Evolution and Environment in Tropical America*, University
592 of Chicago Press. 21-56. [https://doi.org/10.1016/S0169-5347\(97\)89791-1](https://doi.org/10.1016/S0169-5347(97)89791-1)
593
- 594 12. Craig H. 1961. Isotopic variations in meteoric waters. *Science*, 133 (3465): 1702-
595 1703. [DOI: 10.1126/science.133.3465.1702](https://doi.org/10.1126/science.133.3465.1702)
596
- 597 13. Crawford J. et al. 2017. Precipitation stable isotope variability and subcloud
598 evaporation processes in a semi-arid region. *Hydrol. Process.*, 31: 20–34.
599 <https://doi.org/10.1002/hyp.10885>
600
- 601 14. Dansgaard, W. 1964. Stable isotopes in precipitation. *Tellus*. 16, 436-468.
602 <https://doi.org/10.1111/j.2153-3490.1964.tb00181.x>
603
- 604 15. Dee, D.P., et al. 2011. The ERA-Interim reanalysis: Configuration and
605 performance of the data assimilation system. *Quarterly Journal of the royal*
606 *meteorological society*, 137(656): 553-597. <https://doi.org/10.1002/qj.828>
607
- 608 16. Dehaspe, J. et al. 2018. Spatially distributed tracer-aided modelling to explore
609 water and isotope transport, storage and mixing in a pristine, humid tropical
610 catchment. *Hydrological Processes*, 32(21): 3206-3224.
611 <https://doi.org/10.1002/hyp.13258>
612
- 613 17. Delcamp, A., Roberti, G. and van Wyk de Vries, B. 2016. Water in volcanoes:
614 evolution, storage and rapid release during landslides. *Bull. Volcanol.*, 78(87).
615 <https://doi.org/10.1007/s00445-016-1082-8>
616
- 617 18. Dengo, G. 1973. Structural Geology, tectonic history, and morphology of Central
618 America. Centro Regional de Ayuda Técnica, Agencia para el Desarrollo
619 Internacional. <https://searchworks.stanford.edu/view/2739485>
620
- 621 19. Dunn, O. J. 1961. Multiple comparisons among means. *Journal of the American*
622 *Statistical Association*, 56(293): 52-64. [DOI: 10.2307/2282330](https://doi.org/10.2307/2282330)
623

- 624 20. Durán-Quesada A. M. 2012. *Sources of moisture for Central America and*
625 *transport based on a Lagrangian approach: variability, contributions to*
626 *precipitation and transport mechanisms*. PhD Thesis, University of Vigo, Spain.
627 288 pp. <http://www.investigacion.biblioteca.uvigo.es/xmlui/handle/11093/267>.
628
- 629 21. Durán-Quesada, A.M., Gimeno, L. and Amador, J. 2017. Role of moisture
630 transport for Central American precipitation. *Earth System Dynamics*, 8(1): 147-
631 161. <https://doi.org/10.5194/esd-8-147-2017>
632
- 633 22. Esquivel- Hernández, G, Mosquera, GM, Sánchez- Murillo, R, et al. 2018.
634 Moisture transport and seasonal variations in the stable isotopic composition of
635 rainfall in Central American and Andean Páramo during El Niño conditions
636 (2015–2016). *Hydrological Processes*, 33: 1802– 1817.
637 <https://doi.org/10.1002/hyp.13438>
638
- 639 23. Fick, S. E., and Hijmans, R. J. 2017. WorldClim 2: new 1-km spatial resolution
640 climate surfaces for global land areas. *Int. J. Climatol*, 37: 4302-4315.
641 <https://doi.org/10.1002/joc.5086>
642
- 643 24. Food and Agriculture Organization of the United Nations (FAO). 2015. Disaster
644 risk programme to strengthen resilience in the Dry Corridor in Central America.
645 Accessible at: [http://www.fao.org/resilience/resources/resources-](http://www.fao.org/resilience/resources/resources-detail/en/c/330164/)
646 [detail/en/c/330164/](http://www.fao.org/resilience/resources/resources-detail/en/c/330164/). Last accessed: November 12th, 2018.
647
- 648 25. Food and Agriculture Organization of the United Nations (FAO). 2017.
649 Chronology of the Dry Corridor: The impetus for resilience in Central America.
650 Accessible at: <http://www.fao.org/in-action/agronoticias/detail/en/c/1024539/>. Last
651 accessed: November 12th, 2018.
652
- 653 26. Food and Agriculture Organization of the United Nations. 2016. El Niño and La
654 Niña: preparedness and response, situation report July 2016. Accessible at:
655 [http://www.fao.org/emergencies/resources/documents/resources-](http://www.fao.org/emergencies/resources/documents/resources-detail/en/c/423055/)
656 [detail/en/c/423055/](http://www.fao.org/emergencies/resources/documents/resources-detail/en/c/423055/)
657
- 658 27. Foster, S. & MacDonald, A. 2014. The ‘water security’ dialogue: why it needs to
659 be better informed about groundwater. *Hydrogeology Journal*, 22(7): 1489-1492.
660 <https://doi.org/10.1007/s10040-014-1157-6>
661
- 662 28. Fuchs, Ž., Sessions, S.L. and Raymond, D.J., 2014. Mechanisms controlling the
663 onset of simulated convectively coupled Kelvin waves. *Tellus A: Dynamic*
664 *Meteorology and Oceanography*, 66(1): 22107.
665 <https://doi.org/10.3402/tellusa.v66.22107>
666
- 667 29. Giorgi, F. 2006. Climate change hot-spots. *Geophysical research letters*, 33(8).
668 <https://doi.org/10.1029/2006GL025734>

- 669
670
671
672
673
674
675
676
677
678
679
680
681
682
683
684
685
686
687
688
689
690
691
692
693
694
695
696
697
698
699
700
701
702
703
704
705
706
707
708
709
710
711
712
30. González, J. E., M. Georgescu, M. C. Lemos, N. Hosannah, and D. Niyogi. 2017. Climate change's pulse is in Central America and the Caribbean, *Eos*, 98, <https://doi.org/10.1029/2017EO071975>.
 31. Graf, P., Wernli, H., and Sodemann, H. A new interpretative framework for below-cloud effects on stable water isotopes in vapour and rain. *Atmos. Chem. Phys. Discuss.*, <https://doi.org/10.5194/acp-2018-482>, in review, 2018.
 32. Gröning, M. et al. 2012). A simple rain collector preventing water re-evaporation dedicated for $\delta^{18}\text{O}$ and $\delta^2\text{H}$ analysis of cumulative precipitation samples. *J. Hydrology*, 448: 195-200. <https://doi.org/10.1016/j.jhydrol.2012.04.041>
 33. Herrera E, Magaña V, and Caetano E. 2015. Air–sea interactions and dynamical processes associated with the midsummer drought. *Int. J. Climatol.*, 35: 1569-1578. <https://doi.org/10.1002/joc.4077>
 34. Herrera, D. and Ault, T. 2017. Insights from a New High-Resolution Drought Atlas for the Caribbean Spanning 1950–2016. *Journal of Climate*, 30(19): 7801-7825. <https://doi.org/10.1175/JCLI-D-16-0838.1>
 35. Hidalgo, H.G. and Alfaro, E.J., 2015. Skill of CMIP5 climate models in reproducing 20th century basic climate features in Central America. *International Journal of Climatology*, 35(12): 3397-3421. <https://doi.org/10.1002/joc.4216>
 36. Hoekstra, A.Y. et al. 2018. Global food and trade dimensions of groundwater governance. In *Advances in Groundwater Governance* (pp. 353-366). CRC Press-Taylor & Francis group. http://www.fao.org/fileadmin/user_upload/emergencies/docs/FAOEINinoSitRep_versionJULY.pdf. Last accessed: November 12th, 2018.
 37. Houze Jr, R.A. 2004. Mesoscale convective systems. *Reviews of Geophysics*, 42(4). RG4003. <https://doi.org/10.1029/2004RG000150>
 38. Huffman, G.J., et al. 2015. Integrated multi-satellite retrievals for GPM (IMERG), version 4.4. Nat. Aeronaut. Space Admin. (NASA), Washington, DC, USA, NASA's Precipitation Process Center.
 39. Hund, S.V. et al. 2018. Groundwater recharge indicator as tool for decision makers to increase socio-hydrological resilience to seasonal drought. *Journal of Hydrology*. 563: 1119-1134. <https://doi.org/10.1016/j.jhydrol.2018.05.069>
 40. IAEA/WMO: Global Network of Isotopes in Precipitation – the GNIP Database. Accessible at: <https://nucleus.iaea.org/wiser>. Last accessed: 2018-11-20.

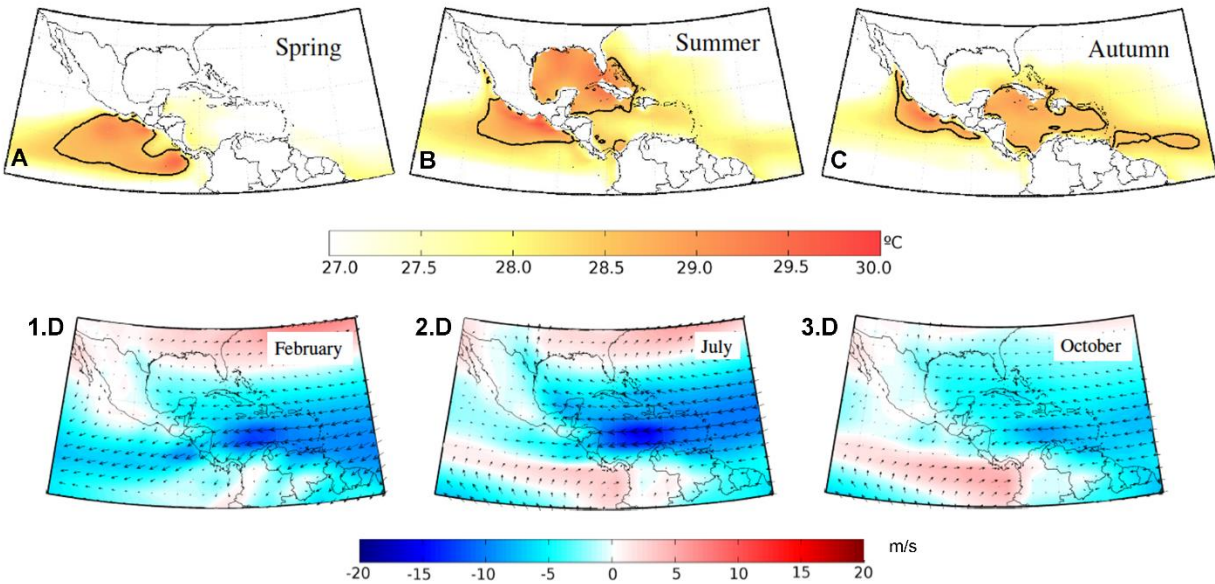
- 713 41. Imbach, P. et al. 2018. Future climate change scenarios in Central America at
714 high spatial resolution. *PloS one*, 13(4), p.e0193570.
715 <https://doi.org/10.1371/journal.pone.0193570>
716
- 717 42. Jasechko, S. and Taylor, R.G. 2015. Intensive rainfall recharges tropical
718 groundwaters. *Environmental Research Letters*, 10(12): 124015.
719 <https://doi.org/10.1088/1748-9326/10/12/124015>
720
- 721 43. Jimenez, J.C. et al. 2018. Spatio-temporal patterns of thermal anomalies and
722 drought over tropical forests driven by recent extreme climatic anomalies.
723 *Philosophical Transactions of the Royal Society B: Biological Sciences*,
724 373(1760): 20170300. <https://doi.org/10.1098/rstb.2017.0300>
725
- 726 44. Knutson, T.R. et al. 2006. Assessment of twentieth-century regional surface
727 temperature trends using the GFDL CM2 coupled models. *Climate*, 19:1624–
728 1651. <https://doi.org/10.1175/JCLI3709.1>
729
- 730 45. Kong, Y. and Pang, Z., 2016. A positive altitude gradient of isotopes in the
731 precipitation over the Tianshan Mountains: effects of moisture recycling and sub-
732 cloud evaporation. *Journal of Hydrology*, 542: 222-230.
733 <https://doi.org/10.1016/j.jhydrol.2016.09.007>
734
- 735 46. Kruskal W. H., and Wallis W. A. 1952. Use of ranks in one-criterion variance
736 analysis. *Journal of the American Statistical Association*, 47(260): 583-621.
737 [DOI:10.2307/2280779](https://doi.org/10.2307/2280779)
738
- 739 47. Leeman, W.P., Carr, M.J., Morris, J.D. 1994. Boron geochemistry of the Central
740 American Volcanic Arc: Constraints on the genesis of subduction-related
741 magmas. *Geochimica et Cosmochimica Acta*, 58(1): 149-168.
742 [http://dx.doi.org/10.1016/0016-7037\(94\)90453-7](http://dx.doi.org/10.1016/0016-7037(94)90453-7).
743
- 744 48. Lyra, A. et al. 2017. Projections of climate change impacts on central America
745 tropical rainforest. *Climatic Change*, 141(1): 93-105.
746 <https://doi.org/10.1007/s10584-016-1790-2>
747
- 748 49. Machado, L.A.T., et al. 1998. Life cycle variations of mesoscale convective
749 systems over the Americas. *Monthly Weather Review*, 126(6):1630-1654.
750 [https://doi.org/10.1175/1520-0493\(1998\)126<1630:LCVOMC>2.0.CO;2](https://doi.org/10.1175/1520-0493(1998)126<1630:LCVOMC>2.0.CO;2)
751
- 752 50. Madrigal-Solís, H., Fonseca-Sánchez, A., and Reynolds-Vargas, J. 2017.
753 Hydrogeochemical characterization of Barva and Colima aquifers in the Central
754 Valley of Costa Rica. *Water Technology and Sciences (in Spanish)*, 8(1), 115-
755 132. <http://www.redacademica.una.ac.cr/display/articulo001126>
756

- 757 51. Magaña, V., Amador, J.A., and Medina, S. 1999. The midsummer drought over
758 Mexico and Central America, *J. Climate*, 12 (1967): 1577-1588.
759 [https://doi.org/10.1175/1520-0442\(1999\)012<1577:TMDOMA>2.0.CO;2](https://doi.org/10.1175/1520-0442(1999)012<1577:TMDOMA>2.0.CO;2)
760
- 761 52. Maldonado, T., Alfaro, E., Fallas-López, B., & Alvarado, L. 2013. Seasonal
762 prediction of extreme precipitation events and frequency of rainy days over Costa
763 Rica, Central America, using Canonical Correlation Analysis. *Advances in*
764 *Geosciences*, 33(33): 41-52. doi:10.5194/adgeo-33-41-2013.
765 <https://doi.org/10.5194/adgeo-33-41-2013>
766
- 767 53. Mapes B.E. et al. 2003. Diurnal patterns of rainfall in northwestern South
768 America. Part I: Observations and context. *Monthly Weather Review*, 131(5):
769 799-812. [http://dx.doi.org/10.1175/1520-0493\(2003\)131<0799:DPORIN>2.0.CO;2](http://dx.doi.org/10.1175/1520-0493(2003)131<0799:DPORIN>2.0.CO;2).
770
771
- 772 54. Maurer, E.P. et al. 2017. Projected twenty-first-century changes in the Central
773 American mid-summer drought using statistically downscaled climate projections.
774 *Regional Environmental Change*, 17(8): 2421-2432.
775 <https://doi.org/10.1007/s10113-017-1177-6>
776
- 777 55. Munksgaard, N.C., Kurita, N., Sánchez-Murillo, R. et al. 2019. Data Descriptor:
778 Daily observations of stable isotope ratios of rainfall in the tropics. *Sci. Rep.*, 9,
779 14419. <https://doi.org/10.1038/s41598-019-50973-9>
780
- 781 56. Muñoz-Jiménez R. et al. Spatial and temporal patterns, trends and
782 teleconnection of cumulative rainfall deficits across Central America. *Int J*
783 *Climatol.*, 1–14. <https://doi.org/10.1002/joc.5925>
784
- 785 57. Poveda, G. and Mesa, O.J. 2000. On the existence of Lloró (the rainiest locality
786 on Earth): Enhanced ocean-land-atmosphere interaction by a low-level
787 jet. *Geophysical research letters*, 27(11): 1675-1678.
788 <https://doi.org/10.1029/1999GL006091>
789
- 790 58. R Core Team (2014). R: A language and environment for statistical computing. R
791 Foundation for Statistical Computing, Vienna, Austria. <http://www.R-project.org/>
792
- 793 59. Ramírez-Leiva, A. et al. 2017. Stable isotopes evidence of recycled subduction
794 fluids in the hydrothermal/volcanic activity across Nicaragua and Costa Rica.
795 *Journal of Volcanology and Geothermal Research*, 345:172-183.
796 <https://doi.org/10.1016/j.jvolgeores.2017.08.013>
797
- 798 60. Reynolds, R.W., et al. 2007. Daily high-resolution-blended analyses for sea
799 surface temperature. *Journal of Climate*, 20(22): 5473-5496.
800 <https://doi.org/10.1175/2007JCLI1824.1>
801

- 802 61. Sáenz F, and Durán-Quesada A. M. 2015. A climatology of low-level wind
803 regimes over Central America using weather type classification approach.
804 *Frontiers in Earth Science*, 3(15):1-18. <https://doi.org/10.3389/feart.2015.00015>
805
- 806 62. Sak, P.B. et al. 2009. Rough crust subduction, forearc kinematics, and
807 Quaternary uplift rates, Costa Rican segment of the Middle American Trench.
808 *Geological Society of America Bulletin*, 121(7-8): 992-1012,
809 <https://doi.org/10.1130/B26237.1>
810
- 811 63. Salamalikis, V., Argiriou, A.A. and Dotsika, E. 2016. Isotopic modeling of the sub-
812 cloud evaporation effect in precipitation. *Science of the Total Environment*, 544:
813 1059-1072. <https://doi.org/10.1016/j.scitotenv.2015.11.072>
814
- 815 64. Sánchez-Murillo et al. 2016b. Isotopic composition in precipitation and
816 groundwater in the northern mountainous region of the Central Valley of Costa
817 Rica. *Isotopes in Environmental and Health Studies*, 53:1, 1-17.
818 <https://doi.org/10.1080/10256016.2016.1193503>
819
- 820 65. Sánchez-Murillo R, and Durán-Quesada A. M. 2018. Preface to Stable isotopes
821 in hydrological studies in the tropics: ecohydrological perspectives in a changing
822 climate. *Hydrological Processes*. <https://doi.org/10.1002/hyp.13305>
823
- 824 66. Sánchez-Murillo R. et al. 2016a. Key drivers controlling stable isotope variations
825 in daily precipitation of Costa Rica: Caribbean Sea versus Eastern Pacific Ocean
826 moisture sources. *Quaternary Sci. Rev.*, 131(Part B): 250-261.
827 <https://doi.org/10.1016/j.quascirev.2015.08.028>
828
- 829 67. Sánchez-Murillo, R. and Birkel, C. 2016. Groundwater recharge mechanisms
830 inferred from isoscapes in a complex tropical mountainous region. *Geophysical*
831 *Research Letters*, 43(10): 5060-5069. <https://doi.org/10.1002/2016GL068888>
832
- 833 68. Sánchez-Murillo, R. et al. 2013. Spatial and Temporal Variation of Stable
834 Isotopes in Precipitation across Costa Rica: An Analysis of Historic GNIP
835 Records. *Open Journal of Modern Hydrology*, 3(4): 226-240. DOI:
836 [10.4236/ojmh.2013.34027](https://doi.org/10.4236/ojmh.2013.34027)
837
- 838 69. Sánchez-Murillo, R., Durán-Quesada, A.M., Esquivel-Hernández, G. et al. 2019.
839 Deciphering key processes controlling rainfall isotopic variability during extreme
840 tropical cyclones. *Nature Commun.*, 10, 4321: doi:10.1038/s41467-019-12062-3.
841 <https://doi.org/10.1038/s41467-019-12062-3>
842
- 843 70. Schneider T, Bischoff T, and Haug GH. 2014. Migrations and dynamics of the
844 intertropical convergence zone. *Nature*, 513(7516): 45-53.
845 <https://doi.org/10.1038/nature13636>
846

- 847 71. Sheffield, J. & Wood, E.F. 2008. Projected changes in drought occurrence under
848 future global warming from multi-model, multi-scenario, IPCC AR4 simulations.
849 *Climate dynamics*, 31(1): 79-105. <https://doi.org/10.1007/s00382-007-0340-z>
850
- 851 72. Stein A. F. et al. 2015. NOAA's HYSPLIT Atmospheric Transport and Dispersion
852 Modeling System. *Bull. Amer. Meteor. Soc.*, 96: 2059–2077. DOI:
853 10.1175/BAMS-D-14-00110.1. <https://doi.org/10.1175/BAMS-D-14-00110.1>
854
- 855 73. Su L. et al. 2015. A comparison of HYSPLIT backward trajectories generated
856 from two GDAS datasets. *Sci. Total Environ.*, 506-507: 527-537.
857 <https://doi.org/10.1016/j.scitotenv.2014.11.072>
858
- 859 74. Taylor, R.G. et al. 2013. Groundwater and climate change. *Nature Climate*
860 *Change*, 3(4): 322. <https://doi.org/10.1038/nclimate1744>
861
- 862 75. Terzer, S. et al. 2013. Global isoscapes for $\delta^{18}\text{O}$ and $\delta^2\text{H}$ in precipitation:
863 improved prediction using regionalized climatic regression models. *Hydrol. Earth*
864 *Syst. Sci.*, 17: 4713–4728. <https://doi.org/10.5194/hess-17-4713-2013>, 2013.
865
- 866 76. Van der Zee Arias, A. et al. 2012. Estudio de caracterización del Corredor Seco
867 Centroamericano (Países CA-4): Tomo I. FAO, Roma (Italia).
868 https://reliefweb.int/sites/reliefweb.int/files/resources/tomo_i_corredor_seco.pdf
869
- 870 77. Villegas P. et al. 2018. Groundwater evolution and mean water age inferred from
871 hydrochemical and isotopic tracers in a tropical confined aquifer. *Hydrological*
872 *Processes*, 32: 2158–2175. <https://doi.org/10.1002/hyp.13160>
873
- 874 78. Wang, C. and Enfield, D.B. 2001. The tropical Western Hemisphere warm
875 pool. *Geophysical research letters*, 28(8): 1635-1638.
876 <https://doi.org/10.1029/2000GL011763>
877
- 878 79. Waylen P. R., Caviedes C.N., and Quesada M.E. 1996. Interannual variability of
879 monthly precipitation in Costa Rica. *J. Clim.* 9:2606-2613.
880 [https://doi.org/10.1175/1520-0442\(1996\)009<2606:IVOMPI>2.0.CO;2](https://doi.org/10.1175/1520-0442(1996)009<2606:IVOMPI>2.0.CO;2)
881
- 882 80. Windhorst, D., Waltz, T., Timbe, E., Frede, H.G. and Breuer, L. 2013. Impact of
883 elevation and weather patterns on the isotopic composition of precipitation in a
884 tropical montane rainforest. *Hydrology and Earth System Sciences*, 17(1): 409-
885 419. <https://doi.org/10.5194/hess-17-409-2013>
886
- 887 81. Zuidema, P., et al. 2006. The interaction of clouds and dry air in the eastern
888 tropical Pacific. *Journal of climate*, 19(18): 4531-4544.
889 <https://doi.org/10.1175/JCLI3836.1>
890
- 891

892
893
894
895
896
897
898



899

900 **Figure 1: Seasonal variations of key regional climate features: WHWP** shown as
901 the area enclosed by the SST > 28.5 isotherm based on Optimum Interpolation Sea
902 Surface Temperature (Reynolds et al., 2007) for A) Spring, B) Summer, C) Autumn and
903 D) CLLJ wind speed shaded contour and wind vector at 925hPa 1.D) February, 2.D)
904 July and 3.D) October from ERA Interim (Dee et al., 2011) long term averages (1998-
905 2017).

906

907

908

909

910

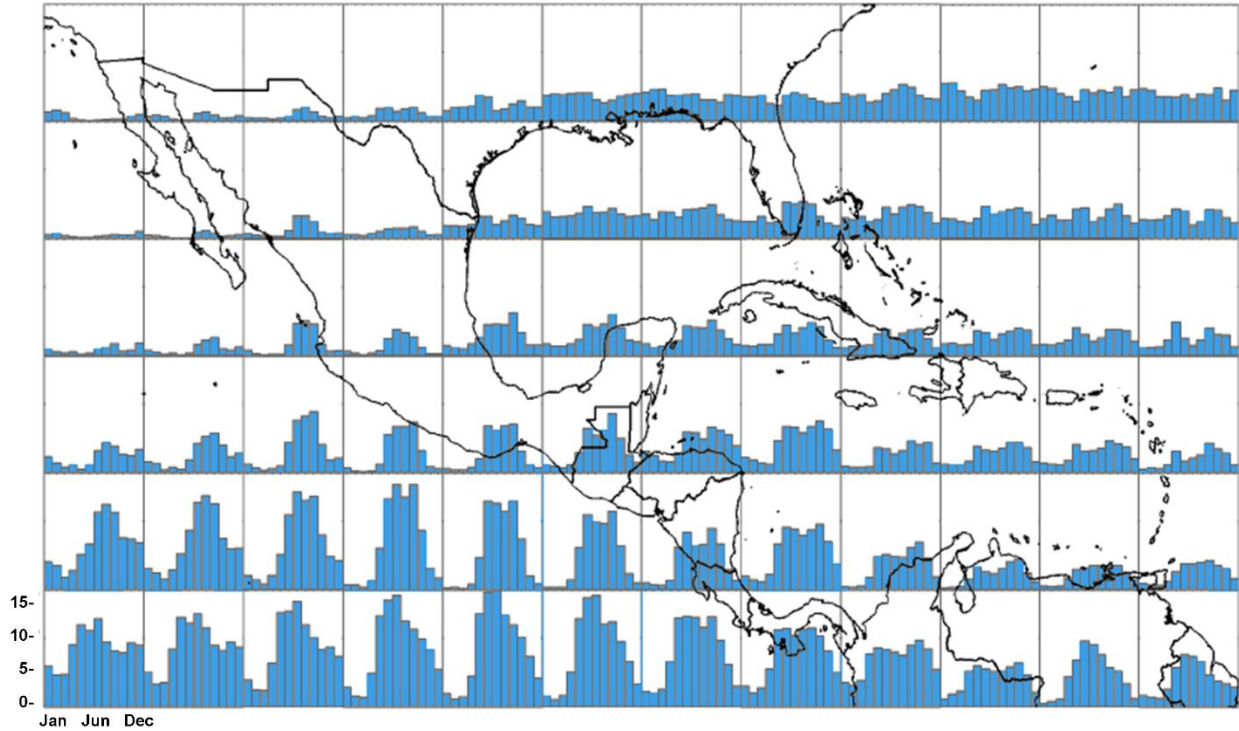
911

912

913

914

915
916
917
918
919
920



921

922 **Figure 2: Spatial and temporal distribution of rainfall across the Central American**
923 **Isthmus.** Climatology distribution of monthly mean precipitation (in mm/day) for
924 contiguous 5x5° area boxes for the 1998-2017 period, estimated using the rainfall
925 product 3B43-7 (Huffman et al., 2014).

926

927

928

929

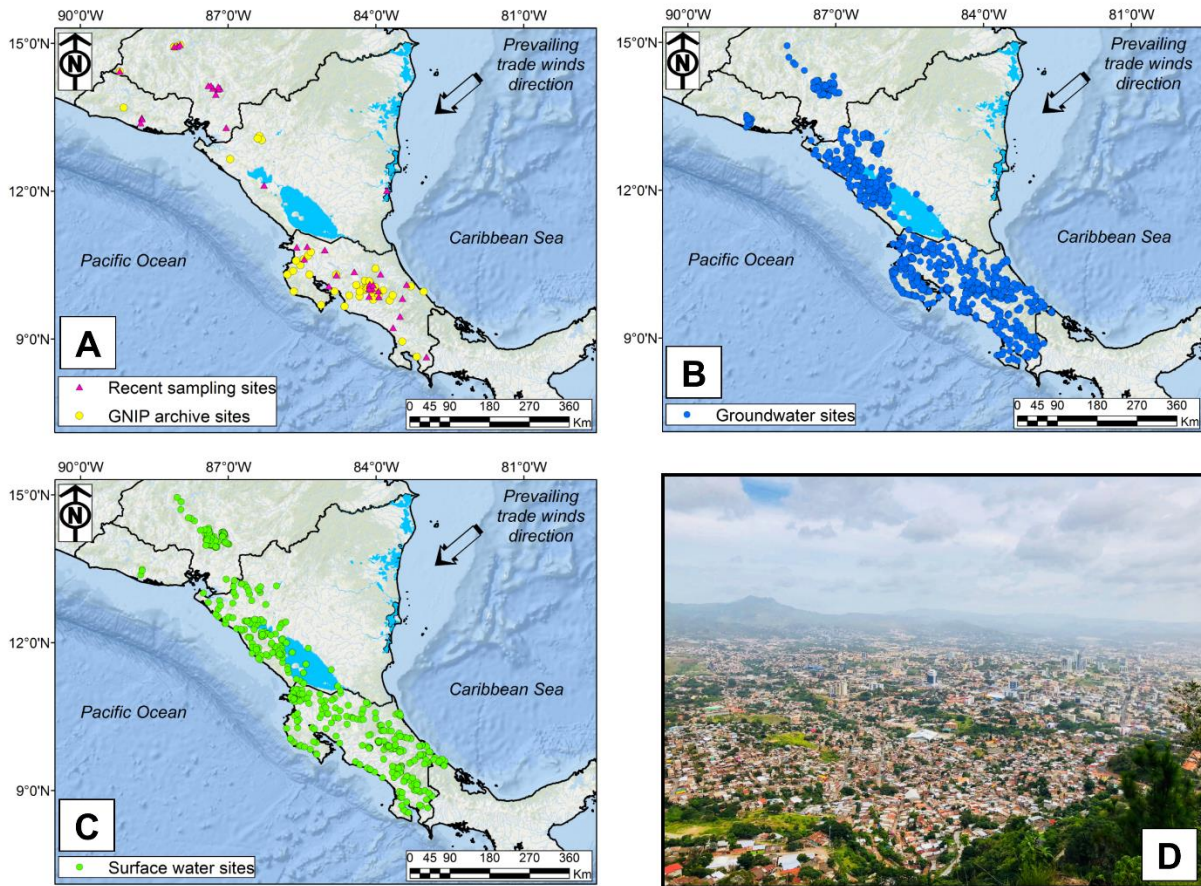
930

931

932

933

934
 935
 936
 937
 938
 939



940
 941
 942
 943
 944
 945
 946
 947
 948
 949
 950
 951

Figure 3: Spatial distribution of rainfall, groundwater, and surface water sampling sites across the Central American Isthmus. A) Recent (2013-2018) rainfall monitoring sites (mostly daily and weekly sampling frequencies; pink triangles) and historical GNP sites (yellow dots). **B)** Distribution of groundwater sampling sites (blue dots). **C)** Distribution of surface water sampling sites (green dots). **D)** Photograph of the highly populated inter-mountainous city of Tegucigalpa, Honduras (Courtesy of RSM). Most cities within the Pacific slope of Central America share a rapid demographic growth coupled with unregulated urbanization within critical recharge elevations.

952
 953
 954
 955
 956
 957
 958
 959
 960
 961
 962
 963
 964
 965
 966
 967
 968
 969
 970
 971
 972
 973
 974
 975
 976
 977
 978
 979
 980
 981
 982
 983
 984
 985
 986
 987
 988
 989
 990
 991
 992
 993
 994
 995
 996
 997

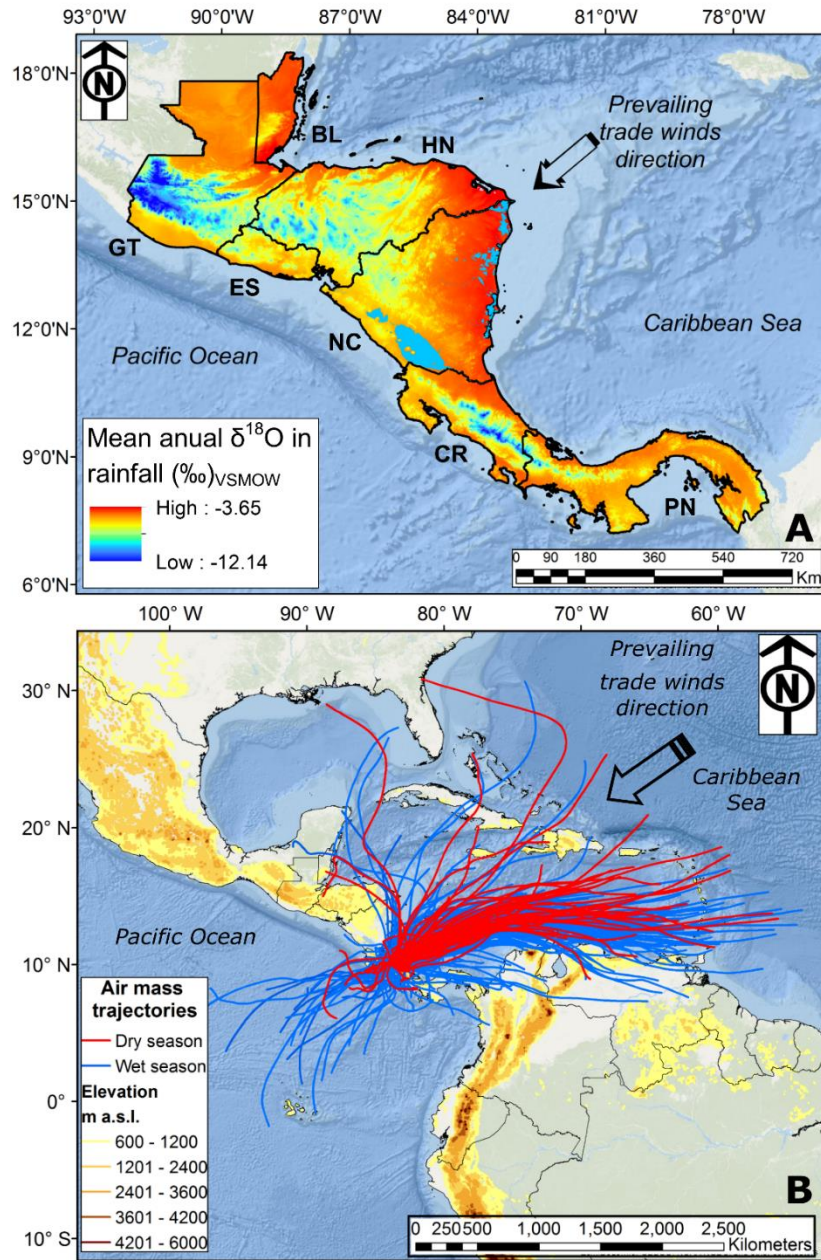


Figure 4: Study area characteristics. A) Regionalized rainfall isoscape within the Central American Isthmus. Mean annual $\delta^{18}\text{O}$ (‰) is color coded. **B)** Representative ($N=476$) dry (red) and wet (blue) seasons 48-hr air mass back trajectories over Costa Rica (2013-2017) using the HYSPLIT Lagrangian model (Stein et al., 2015). Trade winds cross Central America with a NE \rightarrow SW prevailing direction, resulting in notable orographic distillation and complex isotopic spatial variations. (Note: GT=Guatemala; BL=Belize; HN=Honduras; ES=El Salvador; NC=Nicaragua; CR=Costa Rica; PN=Panama).

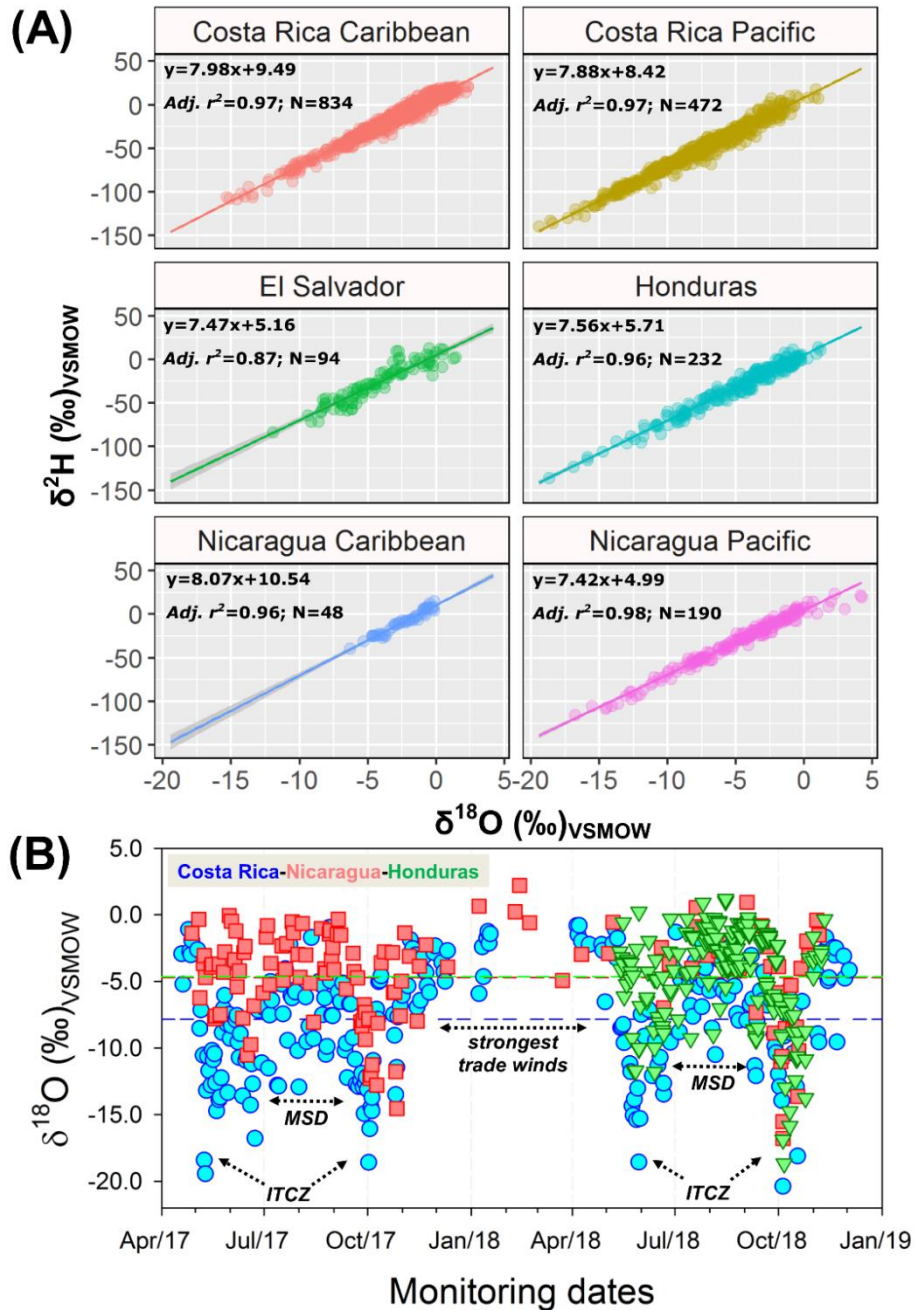
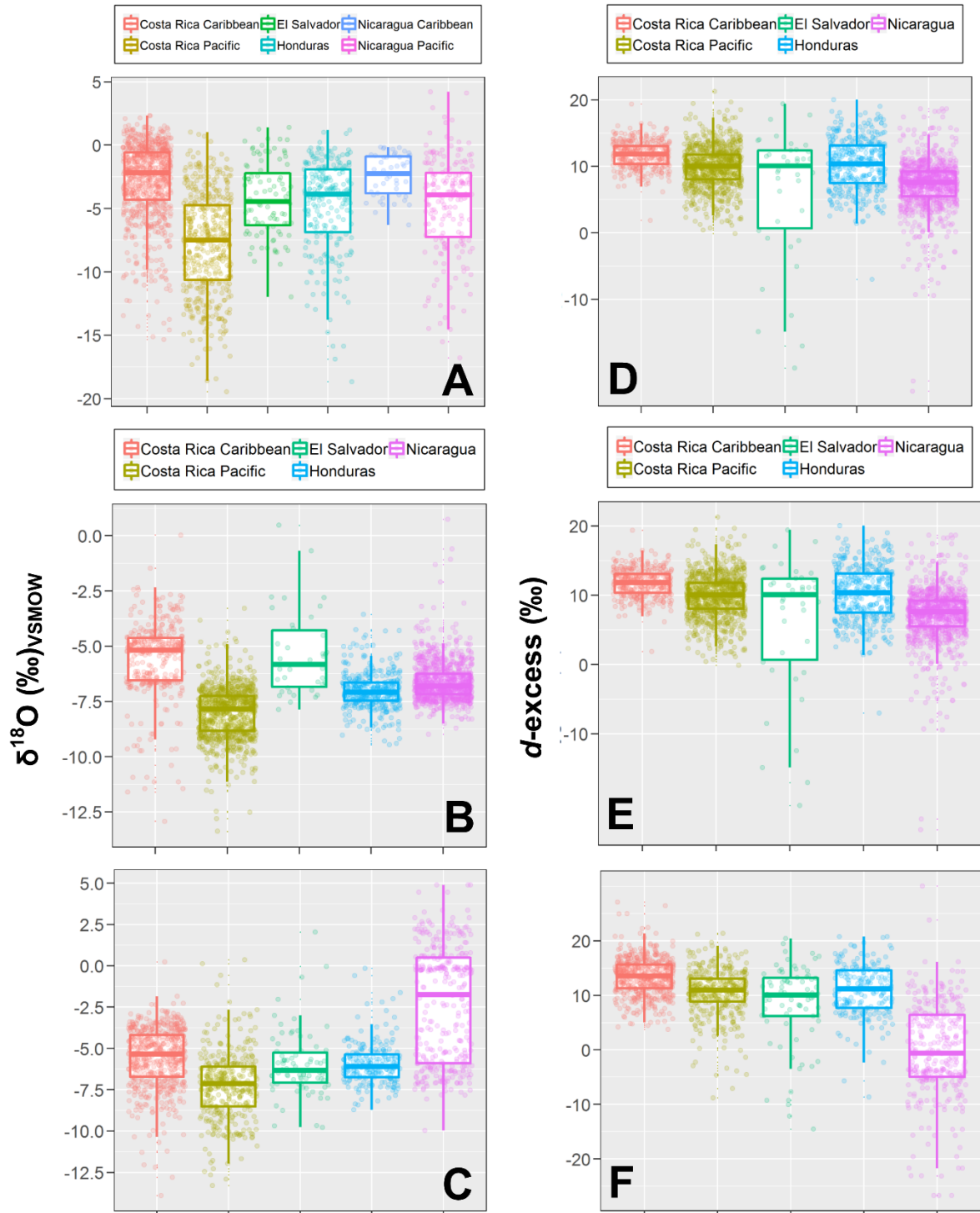


Figure 5: Stable isotope variations of rainfall in Central America. A) Local meteoric water lines (LMWLs) by country and governing rainfall domain (Caribbean versus Pacific). All regressions are significant with a p -value <0.001 . LMWLs include only recent (2013-2018) isotope measurements (mostly daily and weekly sampling frequencies) for comparison purposes. **B)** $\delta^{18}\text{O}$ time series (2016-2018) in Costa Rica, Nicaragua, and Honduras. Horizontal dashed-lines represent the median value of each country. Three main climatic features are related with the isotopic variability in Central America: a) the movement of the ITCZ, b) the MSD, and c) cold fronts during the strongest period of NE trade winds.



1044
 1045
 1046
 1047
 1048
 1049

Figure 6: Scattered and box plots showing variations across the Central American Isthmus (ordered by country and governing rainfall domain) of (A-C) $\delta^{18}\text{O}$ in rainfall, groundwater, and surface water; and (D-F) d -excess in rainfall, groundwater, and surface water, respectively. Box plots include 25th, 75th, median, and outliers for each group.

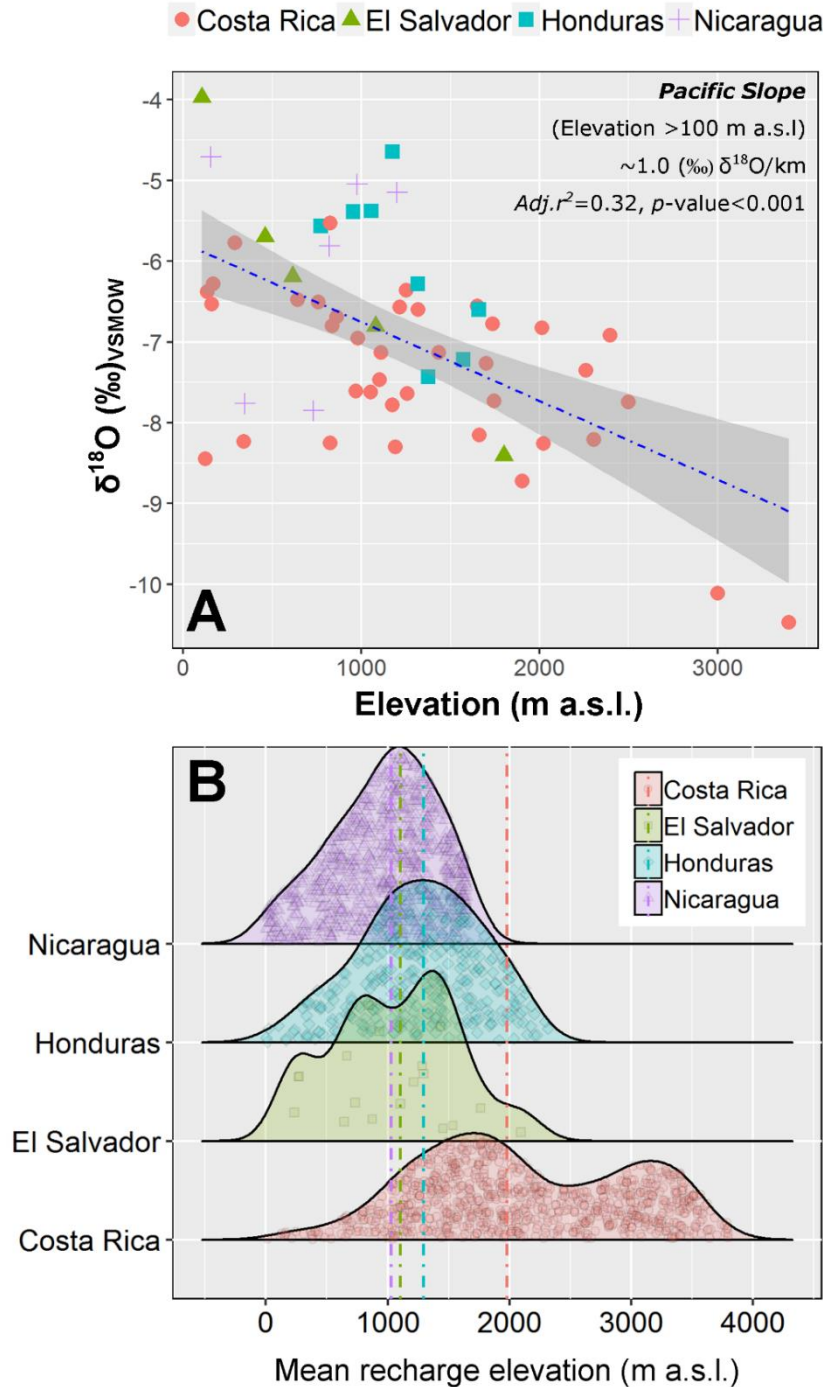
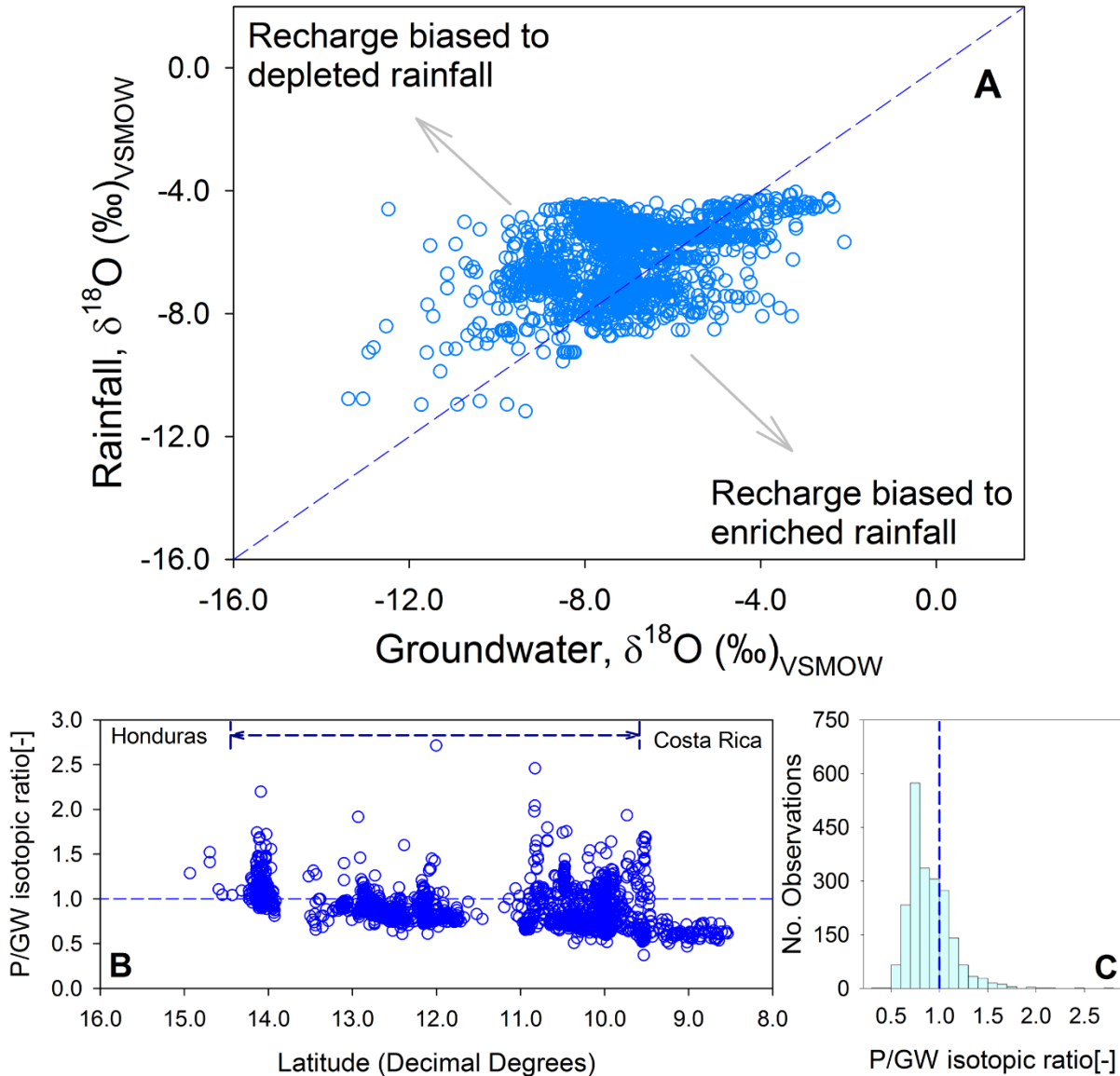


Figure 7: Isotopic lapse rates and potential mean recharge elevations (MRE). A)

Regionalized isotopic lapse rate within the Central American Isthmus using monitoring stations above 100 m a.s.l. Blue dashed-line represents the best linear fit resulting in ~ -1‰ δ¹⁸O per km of elevation gradient with 95% confidence intervals (dark grey area). **B)** Density distribution of MRE (m a.s.l.) by country. Dashed colored-lines denote the median value of each country.



1091

1092

1093

1094

1095

1096

1097

1098

1099

Figure 8: Rainfall and groundwater recharge bias across the Central American Isthmus. **A)** Rainfall and groundwater recharge bias 1:1 diagram following Jasechko and Taylor (2015). **B)** Latitudinal variation of P/GW isotopic ratios [-] from Costa Rica to Honduras. **C)** Histogram of P/GW isotopic ratios [-]. In B and C, the blue dashed-line represents a P/GW=1.